International Journal of Nanoelectronics and Materials
Volume 16, No. 4, October 2023 [749-758]

I-V Characteristics of Polycrystalline CAZTSe Heterojunction Solar Cells at Different Ag Content and Annealing Temperatures

H. I. MOHAMMED[1], Ghuzlan Sarhan Ahmed[1], Seham Hassan Salman[1], Israa Akram Abbas[2] and Sarah M. Obaid [3,*]

[1]Department of Physics, College of Education for Pure Science (Ibn-Alhaitham), University of Baghdad, Baghdad, Iraq.
[2]Department of Physics, College of Education for Pure Science, Al-Mustansiriyah University, Iraq
[3]Technical College of Al-Mussaib, Al-Furat Al-Awsat Technical University, Babylon, Iraq.
Received 3 November 2022, Revised 17 December 2022, Accepted 18 January 2023

ABSTRACT

Since the polycrystalline $(Cu_{1-x}Ag_x)_2ZnSnSe_4$ (CAZTSe) demonstrated good optical absorption performance in the visible region, the focus of the present study is to grow the polycrystalline $(Cu1-xAgx)_2ZnSnSe_4$ thin films deposited by thermal evaporation method on silicon substrates with 800 nm thickness and 0.53 nm/sec deposition rate as a function of Ag content (0.0,0.1,0.2) and annealing temperature at 373 K, 473 K. From I-V measurements of Al/n-CdS/p-CAZTSe/n-Si(111)/Al heterojunction solar cells under dark and illumination conditions, we observed that the forward bias current changes roughly exponentially with bias voltage and the ideality factor and saturation current dependence on both x content and different temperatures (Ta).

Keywords: Polycrystalline CAZTSe, Ag content and annealing temperature, I-V characteristics

1. INTRODUCTION

In the past decades, two thin film technologies based on CdTe and $CuInGaSe_2$ (CIGS) have appeared [1,2]. These devices have achieved conversion efficiency exceeding 20% [3,4]. Although this type of solar cell has reached the commercial producing stage [5], the scarcity and cost of Te and In, in addition to the toxicity of Cd [6,7], have limited their widespread utilization [8]. Therefore, researchers have focused on finding alternate absorber layers of available and nontoxic materials [2,9]. So, they substitute the rare earth indium (In) and gallium (Ga) in the CIGS compound with zinc (Zn) and tin (Sn) with appropriate stoichiometry to get copper zinc tin sulfide (CZTS) or selenide (CZTSe) [10]. $Cu_2ZnSnSe_4$ has drawn important interest due to its coefficient of high absorption, p-type conductivity, suitable direct band gap, as well as earth-abundant and nontoxic component elements [11,12]. Although CZTSe based solar cells have achieved high photo conversion efficiency, they remain lag behind commercial solar cells because of the limited open circuit voltage (V_{oc}) [13]. To increase the V_{oc} value, the density of defects in CuZn antisite acceptors must be reduced by replacing Cu with a larger element. Although Ag is considered not an earth-abundant element, it is an important candidate to replace Cu because its atomic radius is about 16% larger and belongs to the same chemical group [14]. The original material's band gap will be altered by this process, but the crystal structure and cation coordination will remain unchanged [15]. Henry *et al*. [16] analyzed the properties of vacuum-evaporated Cu_2ZnSnS_4 (CZTSe), $CuAgZnSnS_4$ (CAZTSe), and Ag_2ZnSnS_4 (AZTSe) thin films. They confirmed a peak shift toward the lower angle for CAZTSe and AZTSe films in the presence of tetragonal-structured CZTSe. Higher mobility was shown by the CAZTSe film, which is advantageous for solar applications. Sa and Liu [17] investigated the structural, mechanical, electronic, and optical properties of $(Cu_{1-x}\ Ag_x)\ 2SnZnSe_4$ (CAZTSe) solid solutions

* Corresponding author: sarah.obaid.cnj@atu.edu.iq

theoretically. From their study, they confirm the mechanical stability of each compound. Thin film solar cells made of $CuAgZnSnSe_4$ (CAZTSe) were created on a variety of conducting substrates (Al, Cu, Ag, FTO, and AZO). Henry et al. fabricated conducting substrates (Al, Cu, and Ag) *via* vacuum evaporation [18] and then produced CAZTSe thin films on both commercial and non-commercial (FTO and AZO) substrates using the same technique. The CAZTSe films' band gap ranged from 1.514 to 1.893 eV. All of the films had n-type conductivity, according to Mott-Schottky plots, and the carrier concentration was in the 10^{18}–10^{19} cm^{-3} ranges. Mora-Herrera and Pal [19] argued that a tandem solar cell made of monolithic kesterite can absorb light across a broad spectral range. Cu2ZnSnS4 (CZTS) top cell with a greater band gap and an underlying $(Ag_xCu_{1-x})_2ZnSnSe_4$ (ACZTSe) bottom cell with a smaller band gap make up the suggested tandem structure. They are coupled in a series circuit via a tunnelling junction.

The goal of the present study is to deposit polycrystalline $(Cu_{1-x}Ag_x)_2ZnSnSe_4$ thin films on silicon substrates with 800 nm thickness and 0.53 nm/sec deposition rate as a function of Ag content (0.0,0.1,0.2) and annealing temperature (373, 473) K using the thermal evaporation technique. The I-V characteristics of the prepared films will be measured and discussed.

2. EXPERIMENTAL PROCEDURE

The CAZTSe HJs solar cells were fabricated, and the single-crystal silicon wafer substrates were used. These substrates were carefully cleaned by using several methods depending on the type of substrate. A thin layer of Al was deposited on the anti-reflected face of the Si wafer as a back electrode for HJs. The required amount of $(Cu_{1-x}Ag_x)_2ZnSnSe_4$ powder, which depends on the value of x to achieve the desired thickness of 800 nm, was located in a molybdenum boat tied in the vacuum chamber between two electrodes. When the system was pumped down to 10^{-5} Torr, the Si/Al substrates were fixed to the substrates holder and positioned at a height of 18 cm above the boat. When the boat reached the required temperature, the deposition process began with a 0.53 nm/sec deposition rate after an electric current was gradually passed through it. After all the material evaporated, the current was gradually reduced to zero. The same steps were used to deposit thin CdS films with 100 nm and 0.3 nm/sec deposition rate on CAZTSe/Si/Al structures using CdS powder, which was provided by Balzers (company) with a high purity of 99.999%. The deposited films were left under high vacuum for one day. Some of the prepared samples were annealed at 373 K and 473 K under vacuum for 1 h using an electrical furnace. In the last step to complete the fabrication of the HJ solar cells, suitable electrodes were deposited on the CdS/CAZTSe/Si/Al structures of Al metal using a suitable mask.

A 70 nm CdS buffer layer, deposited via a chemical bath, completes the solar cells. The samples are submerged in a solution containing ammonium acetate (20 mM), thiourea (5.1 mM), cadmium acetate (1 mM), and ammonia (0.3 mM) for 15 minutes while being agitated at 600 rpm. In an MRC2 chamber, the 50 nm/250 nm i-ZnO/ZnO:Al (Al2O3 2 at%) window layer is RF-sputtered without purposeful sample heating. Thermal evaporation is used to create Ni (50 nm) and Al (500 nm) grids on top of the solar cell. Each sample has at least ten hands inscribed 0.5 x 0.5 cm^2 solar cells.

Finally, the front and back Al electrodes were connected to the appropriate wires for carrying out the electrical measurements of the cell. Under light irradiation, the open circuit voltage (Voc), short circuit current (Isc), maximum power point (Pm), fill factor (F.F.), and photovoltaic conversion efficiency (PCE, η) were estimated from the I-V measurements. The fill factor and photovoltaic conversion efficiency were estimated using standard equations [20, 21]:

$$F.F. = \frac{P_{max}}{V_{oc}I_{sc}} = \frac{V_{max}\ I_{max}}{V_{oc}I_{sc}} \quad (1)$$

$$\eta = \frac{P_{max}}{P_{in}} * 100\% = \frac{F.F.\ V_{oc}\ I_{sc}}{P_{in}} * 100\ \% \quad (2)$$

From I-V measurements in the dark, the major diode parameters were evaluated, such as ideality factor (β) and saturation current (Is). The ideality factor was obtained by using the following relation [20]:

$$\beta = \frac{q}{k_B T}\left[\frac{V_f}{Ln(I_f/I_s)}\right] \quad (3)$$

where q is the charge of an electron, T stands for the absolute temperature, KB for the Boltzmann constant, and V_f for the forward bias voltage., and if denotes the forward bias current. Black box and Halogen lamp light of (40 mW/cm^2) power density (Pin) was used to obtain dark and light (I-V) measurements, respectively, under forward and reverse bias.

3. RESULTS AND DISCUSSION

One of the crucial characteristics of the junction is the current-voltage curve, which depicts how the resulting current behaves with applied forward and reverses bias voltage [21]. Figure 1 depicted the I-V characteristics curve of the prepared Al/CdS/(Cu1-xAgx)2ZnSnSe4/Si/Al HJ solar cells at RT with various Ag content of 0 (panels a, b,c), 0.1 (panels d, e, f), and 0.2 (panels g, h, i) and annealing temperatures (373 and 473) K at forward and reverse bias voltage in the dark and illumination conditions. In general, the applied voltage injects the majority carrier, which causes the forward dark current, reducing the built-in potential and the depletion region's width [22]. Then, the majority and minority carrier concentrations are higher than the intrinsic carrier concentration, i.e. pn>ni^2 leading to generating a recombination current in the low voltage region (0-0.3 volt). However, the tunnelling current is resented in the high voltage region (0.3 V). Following that, the current value rapidly increases exponentially as the voltage increases, known as the diffusion current [23, 24]. The reverse bias current includes two regions. The first region is the generation current, which depends on the bias voltage. The width of the depletion region and the generation current both increase as the bias voltage rises. While in the second region, the reverse bias current stabilizes and becomes independent of the bias voltage in the diffusion current [25]. It can be seen from Figure 1 that the behavior of the current under illumination at forward and reverse bias voltage is similar to that of the dark current with an apparent increase in the current value. During the cell illumination, photons with energies equal to or greater than the CAZTSe band gap energy are absorbed by semiconductors. This creates e-h pairs in the depletion region, which are separately driven at the interface by the electric field [26]. Another observation is that the illumination current increases when x content and Ta increase due to the improvement in the film depletion region width, film absorbance, carrier mobility, and film crystal structure with increasing x value and Ta.

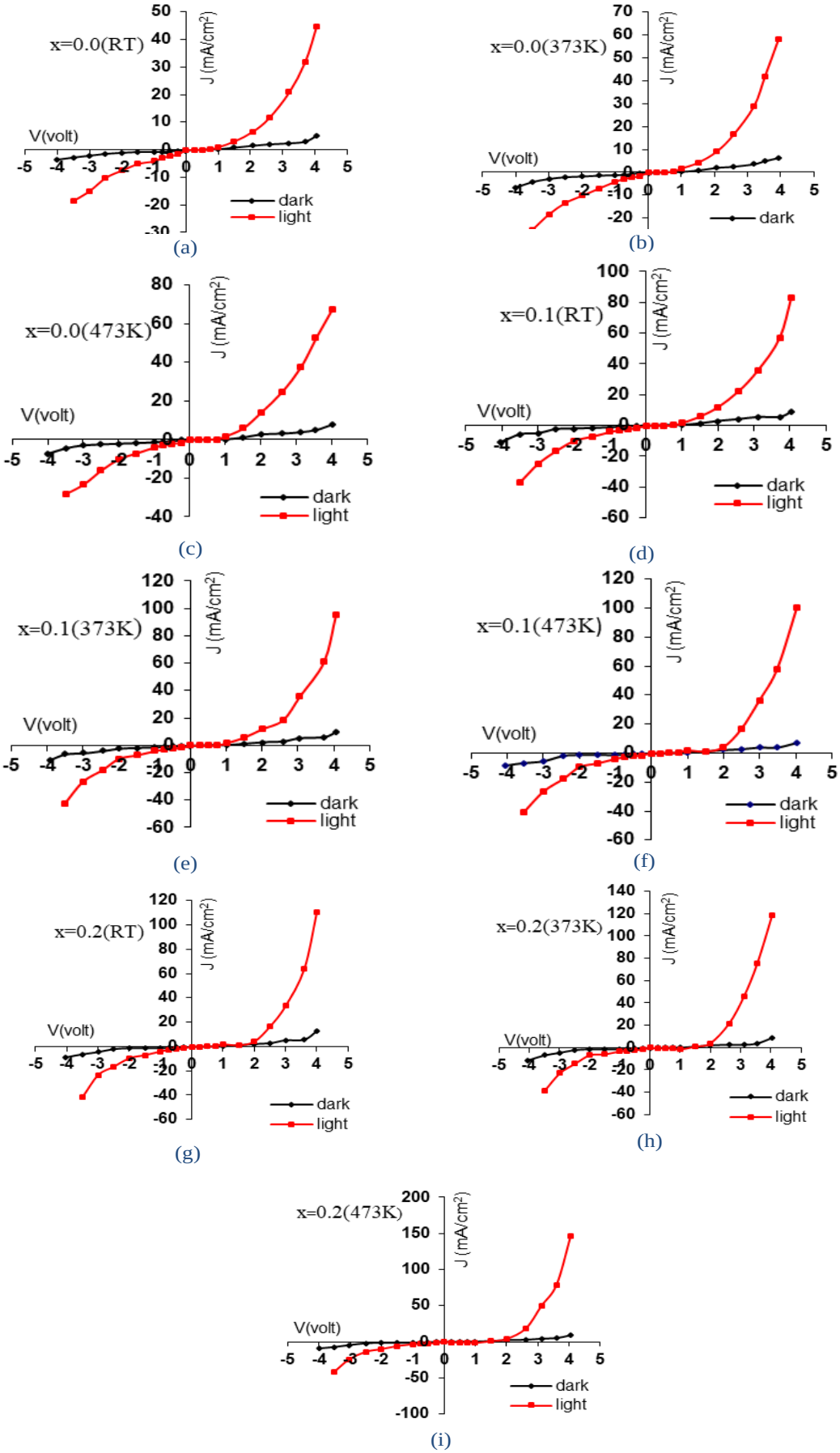

Figure1: I-V characteristics under dark and illumination for Al/CdS/(Cu1-xAgx)2ZnSnSe4/Si/Al

HJ solar cells with various x content and Ta.

The parameters open circuit voltage (Voc) and short circuit current (Isc) are essential because they can identify the region where the heterojunction operates. The magnitude of Vm (maximum voltage) and Im (maximum current) are estimated at the maximum power point on the photovoltaic power output curve as seen in Figure 2 with Ag content for 0 (panels a, b,c), 0.1 (panels d, e, f), and 0.2 (panels g, h, i). The fill factor and efficiency, calculated by using Eqs. (1) and (2), respectively. The results are summarized in Table 1. The data shows that the values of Voc and Isc increased as the x value and Ta increased, which in turn increased the Vmax, Imax, and the F.F. This may be attributed to the improvement in the absorber layer properties with increasing x content and Ta. It is also noticed that the photoconversion efficiency (PCE) of the cell increases with increasing x content and Ta. This may be due to an increase in the particle size of the absorber layer with increasing Ag content and Ta. Because the minority carrier diffusion length and built-in potential are both maximized by large particle size in the absorber layer, the PCE of the constructed cell is significantly correlated with particle size [27, 28]. The rise in PCE can also be related to the expansion of the depletion region [29, 30]

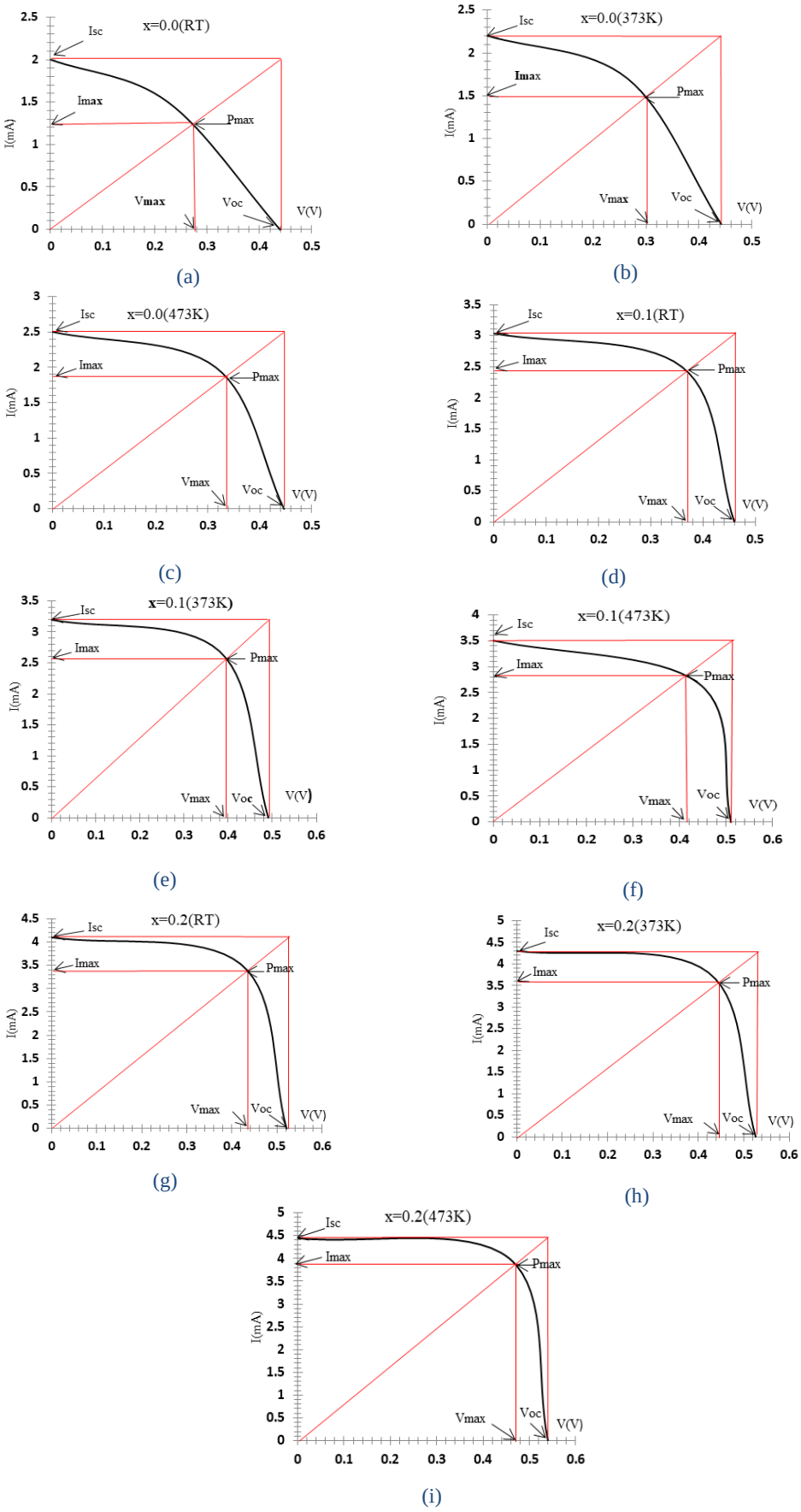

Figure 2: I_{sc} and Voc curves for Al/CdS /CAZTSe/Si/Al HJs solar cells with various x values and Ta

Table 1. The values of Isc, Voc, Imax, Vmax, F.F and efficiency (η %) for Al/CdS/(Cu1-xAgx)2ZnSnSe4/Si/Al HJs solar cells with various x value and Ta.

x	T_a(K)	I_{sc} (mA)	V_{oc} (V)	I_{max} (mA)	V_{max} (V)	F.F.	η%
0	RT	2	0.44	1.23	0.275	0.3844	**0.529**
	373	2.2	0.442	1.5	0.31	0.4782	**0.727**
	473	2.5	0.447	1.87	0.335	0.5606	**0.979**
0.1	RT	3.04	0.46	2.43	0.37	0.6429	**1.405**
	373	3.2	0.49	2.56	0.398	0.6498	**1.592**
	473	3.5	0.51	2.82	0.413	0.6525	**1.82**
0.2	RT	4.1	0.52	3.38	0.433	0.6865	**2.287**
	373	4.3	0.527	3.6	0.442	0.7022	**2.486**
	473	4.44	0.54	3.85	0.47	0.7547	**2.827**

Figure 3 shows the relations between the forward dark current logarithm as a function of applied voltage (0-1) V for prepared Al/CdS/(Cu1-xAgx)2ZnSnSe4/Si/Al photovoltaic cells at RT with various Ag content for 0 (panels a, b,c), 0.1 (panels d, e, f), and 0.2 (panels g, h, i) and annealing temperatures 373K and 473K. This data shows that the forward current consists of two regions. The first region represents the recombination current due to an increase in the carrier at low bias. In contrast, the second region represents the tunnelling current due to a decrease in the width of the depletion region with increasing the bias voltage, resulting in an increase in the chance of carrier tunnelling. From the first region, the ideality factor (β) of the prepared HJs was calculated using Eq. (3), and the obtained results are listed in Table 2. The physical meaning of the ideality factor being greater than 2 is that the tunnelling plays a significant role in the recombination-emission [31]. The value of the diode ideality factor is a key aspect for diagnosing the type of recombination and its location within the device [32]. As shown in Table 2, the value of the ideality factor is greater than unity (β>1), which means that the dark current results from the non-ideal recombination of electrons and holes in the space charge region. The reverse saturation current (Is) for all samples is determined from the intercept of the straight line with the current axis at zero bias voltage, as seen in Figure 3, and the obtained data are listed in Table 2. The decreased values of β and Is with increasing x content and Ta indicate the improvement in the crystal structure and the reduction of the defects that act as active recombination centres, resulting in lower recombination rates for the e-h pairs and improved solar cell performance.

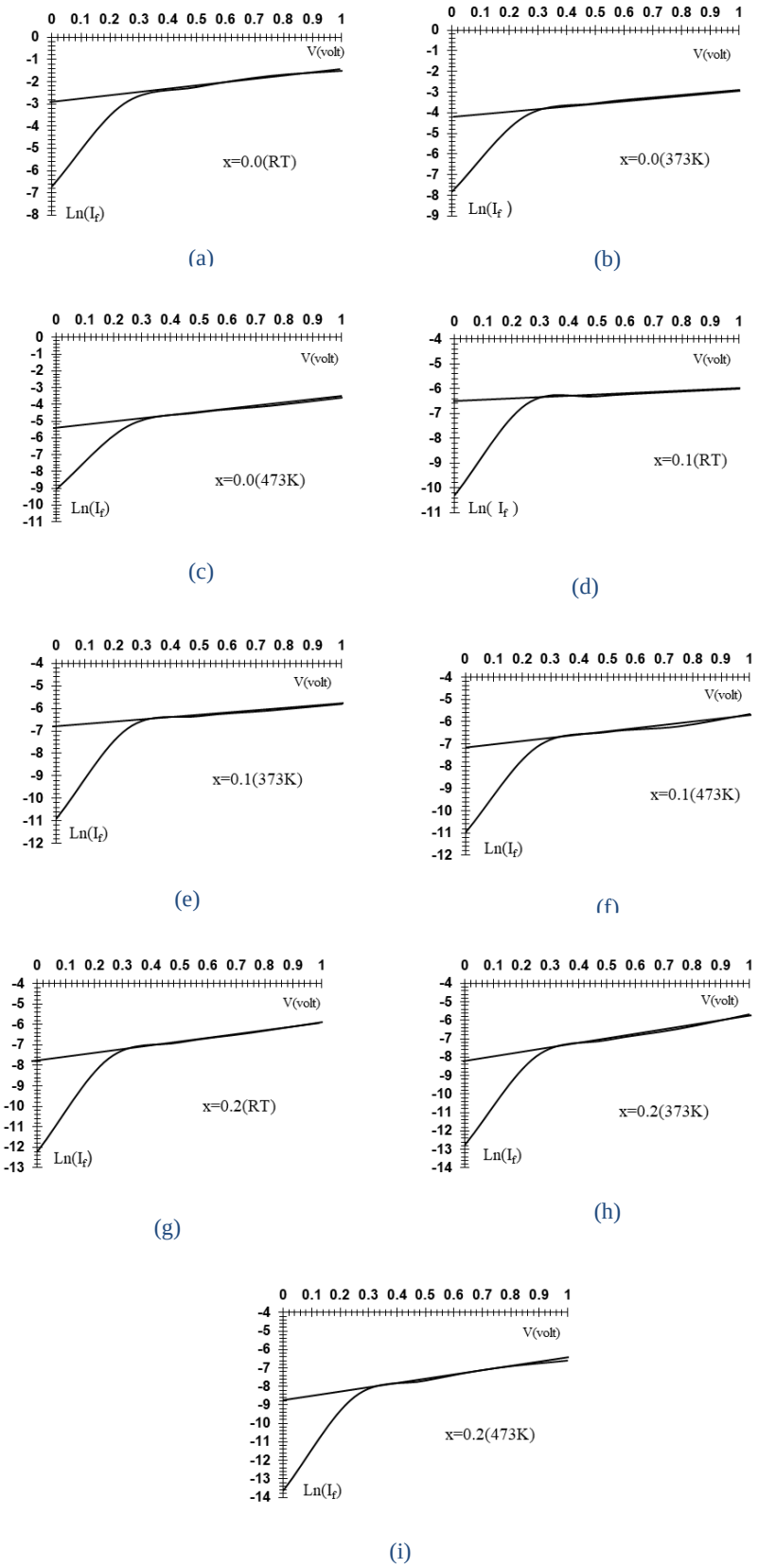

Figure 3: Ln(I) as a function of V for dark forward bias for Al/CdS/(Cu1-xAgx)2ZnSnSe4/Si/Al HJs solar cells with various x values and Ta.

Table 2: Values of ideality factor and saturation current for CdS/CAZTSe/Si HJs solar cells for different x content and Ta.

x	Ta(K)	Ideality factor (β)	Saturation current (I_s) mA
0	RT	3.0351	0.055
	373	3.0059	0.015
	473	2.9566	0.0045
0.1	RT	2.8402	0.0015
	373	2.7969	0.00011
	473	2.7459	0.00074
0.2	RT	2.5472	0.00041
	373	2.4686	0.00027
	473	2.3993	0.00015

4. CONCLUSION

In this study, I-V characteristics under illumination showed that the performance of the manufactured solar cell improved with increasing x value and Ta. Therefore, the optimum conditions in which the cell will operate for best performance (F. F=0.7547 and η= 2.827%) are when the x value and Ta equal to 0.2 and 473K, respectively. I-V measurements under dark with forward bias for all prepared Al/CdS/CAZTSe/Si/Al HJs showed that the values of the demonstrated that as x content and Ta increased, the values of the ideality factor and saturation current decreased.

REFERENCES

[1] Guo, H., Ma, C., Zhang, K., Jia, X., Li, Y., Yuan, N., & Ding, J., Solar Energy Materials and Solar Cells, vol **178**, (2018) pp.146-153.
[2] Green, M.A., Progress in Energy, vol **1**(1) (2019) p.013001.
[3] Friedlmeier, T.M., Jackson, P., Bauer, A., Hariskos, D., Kiowski, O., Menner, R., Wuerz, R. and Powalla, M., Thin Solid Films, vol **633** (2017) pp.13-17.
[4] Tina, G.M., Scavo, F.B., Merlo, L. and Bizzarri, F., Applied Energy, vol **281** (2021) p.116084.
[5] Mansfield, L.M., Kanevce, A., Harvey, S.P., Bowers, K., Beall, C., Glynn, S. and Repins, I.L Progress in Photovoltaics: Research and Applications, vol **26**(11) (2018) pp.949-954.
[6] Exarhos, S., Palmes, E., Xu, R. and Mangolini, L RSC advances, vol **7**(41) (2017) pp.25575-25581.
[7] Lai, F. I., Yang, J. F., Wei, Y. L., & Kuo, S. Y., vol.**19**, issue 3(2017)795-802.
[8] Fthenakis, V., Athias, C., Blumenthal, A., Kulur, A., Magliozzo, J., & Ng, D, Renewable and Sustainable Energy Reviews, vol. **123**, (2020) pp.109776.
[9] Kuo, D. H., & Wu, H. P., Advanced Materials Research, vol. **463**, (2012). pp. 602-606.
[10] Simya, O. K., Priyadarshini, B. G., Balachander, K., & Ashok, A. M., Materials Research Express, vol **7**, issue 1, (2020) pp. 016419.

[11] Kim, J., Park, S., Ryu, S., Oh, J. and Shin, B.,Progress in Photovoltaics: Research and Applications, vol. **25**(4) (2017)pp.308-317.
[12] Wang, A., Chang, N.L., Sun, K., Xue, C., Egan, R.J., Li, J., Yan, C., Huang, J., Rong, H., Ramsden, C. and Hao, X., Sustainable Energy & Fuels, vol **5**(4) (2021) pp.1044-1058.
[13] Gershon, T., Sardashti, K., Lee, Y. S., Gunawan, O., Singh, S., Bishop, D., & Haight, R., Acta Materialia, vol **126** (2017) pp. 383-388.
[14] Goktas, A., Tumbul, A. and Aslan, F., Journal of Sol-Gel Science and Technology, vol **90**(3) (2019.) pp.487-497.
[15] Mohammed. H. I., Ph.D. thesis, University of Baghdad (2021).
[16] Henry, J., Sivakumar, G., Vettumperumal, R., Subramanian, T. and Mohanraj, K., Materials in Electronics, vol **32**(15) (2022) pp.20259-20272.
[17] Sa, R. and Liu, D., Materials Chemistry and Physics, vol **279** (2022) p.125757.
[18] Henry, J., Mohanraj, K. and Sivakumar, G., . Vacuum, vol 160 (2019) pp.347-354.
[19] Mora-Herrera, D. and Pal, M., Physica E: Low-dimensional Systems and Nanostructures, vol. **138** (2022) p.115056.
[20] Bayod-Rújula, A.A., Solar photovoltaics (PV). In Solar Hydrogen Production (pp. 237-295). Academic Press. (2019).
[21] Siu, C., Semiconductor physics. In Electronic Devices, Circuits, and Applications (pp. 35-39). Springer, Cham. (2022).
[22] Fdhala, M., Hemed, A., Al-Ansari, R., Al-Haddad, R. and Abbas, R., Kuwait Journal of Science, vol **49**(2) (2022).
[23] Sze, S. M., & Ng, K. K., 3rd ed. John Wiley & Sons: Hoboken NJ, USA, (2007)134-196.
[24] Kittel, C. and McEuen, P., Introduction to solid state physics. John Wiley & Sons, (2018).
[25] Lee, M., Ryu, H.Y., Ko, E. and Ko, D.H., ACS Applied Electronic Materials, vol. **1**(3) (2019) pp.288-301.
[26] Shelke, H. D., Lokhande, A. C., Patil, A. M., Kim, J. H., & Lokhande, C. D., Surfaces and Interfaces, vol **9**, (2017) pp. 238-244.
[27] Henry J., Mohanraj K., Sivakumar G., Vacuum J., vol **156**, (2018) pp.172-180.
[28] Henry, J., Mohanraj, K., & Sivakumar, G., Vacuum, vol **160** (2019) pp.347-354.
[29] Henry J., Mohanraj K., Sivakumar G., J. Phys. Chem. C **123**, (2019) pp.2094.
[30] Zhan, L., Ning, X., Zhou, X., Luo, J. and Fan, X., 2022. Advanced Powder Technology, vol. **33**(4) (2022) p.103521
[31] Lee, J.H., Hiramoto, M. and Izawa, S. Japanese Journal of Applied Physics, vol. **61**(1) (2021) p.011001.
[32] Courtier N. E., Phys. Rev. Applied, vol **14**, (2020) pp. 024031.
[33] Meyer E. L, International Journal of Photoenergy, vol **2017**, (2017).